Revealing intact neuronal circuitry in centimeter-sized formalin-fixed paraffin-embedded brain

Ya-Hui Lin, Li-Wen Wang, Yen-Hui Chen, Yi-Chieh Chan, Shang-Hsiu Hu, Sheng-Yan Wu, Chi-Shiun Chiang, Guan-Jie Huang, Shang-Da Yang, Shi-Wei Chu, Kuo-Chuan Wang, Chin-Hsien Lin, Pei-Hsin Huang, Hwai-Jong Cheng, Bi-Chang Chen & Li-An Chu**

Y. H. Lin, L. W. Wang, Y. C. Chan, Prof. S. H. Hu, S. Y. Wu, Prof. C. S. Chiang, Prof. L. A. Chu
Department of Biomedical Engineering and Environmental Sciences
National Tsing Hua University
Hsinchu, 300044, Taiwan
E-mail: lachu@mx.nthu.edu.tw

Y. H. Lin, L. W. Wang, Prof. L. A. Chu
Brain Research Center
National Tsing Hua University
Hsinchu, 300044, Taiwan

Prof. Y. H. Chen
Institute of Biomedical Sciences
Academia Sinica
Taipei, 115024, Taiwan

G. J. Huang, Prof. S. W. Chu
Department of Physics
National Taiwan University
Taipei, 106216, Taiwan

Prof. S. D. Yang
Institute of Photonics Technologies
National Tsing Hua University
Hsinchu, 300044, Taiwan

Dr. Kuo-Chuan Wang
Department of Neurosurgery
National Taiwan University Hospital
Taipei, 100225, Taiwan

Dr. Chin-Hsien Lin
Department of Neurosurgery
National Taiwan University Hospital
Taipei, 100225, Taiwan

Dr. Pei-Hsin Huang
Department of Pathology
National Taiwan University Hospital
Taipei, 100225, Taiwan

Prof. Hwai-Jong Cheng

Institute of Molecular Biology
Academia Sinica
Taipei, 115024, Taiwan

Prof. Bi-Chang Chen
Research Center for Applied Sciences
Academia Sinica
Taipei, 115024, Taiwan
E-mail: chenb10@gate.sinica.edu.tw

Keywords: tissue clearing, multiplexed staining, formalin-fixed paraffin-embedded, archived tissues, whole-mouse brain imaging

Abstract

Tissue clearing and labeling techniques have revolutionized brain-wide imaging and analysis, yet their application to clinical formalin-fixed paraffin-embedded (FFPE) blocks remains challenging. We introduce MOCAT, a novel method for efficiently clearing and labeling centimeter-thick FFPE specimens using elevated temperature and concentrated detergents. MOCAT with multi-round immunolabeling reveals neuron circuitry regulating multiple neurotransmitter systems in a whole FFPE mouse brain, and is able to be used as the evaluation of disease treatment efficiency. MOCAT also supports expansion microscopy and can be performed on a non-sectioned 15-year-old FFPE specimen. Thus, MOCAT represents a feasible approach for researching archived FFPE specimens for future neuroscientific and 3D neuropathological analyses.

1. Introduction

Clinical brain tissues play a critical role in unraveling the molecular mechanisms underlying neurological diseases and facilitating the development of effective treatments,[1–3] and also represent an invaluable resource for retrospective studies on rare diseases or conditions with long-term outcomes.[4] Currently, the majority of archived clinical specimens are stored in the form of formalin-fixed paraffin-embedded (FFPE) blocks. Advanced molecular analysis tools—such as chromatin immunoprecipitation (ChIP), DNA/RNA sequencing (DNA/RNA-seq), and Luminex assays—have been performed on FFPE specimens to enable comprehensive analysis from genomic, transcriptional, and proteomic perspectives.[3,5–7] However, image-based qualification and quantification of FFPE samples remains limited to performing chemical staining and immunohistochemistry on thin sections. Although whole-slide imaging enables unbiased analyses of entire tissue sections,[3,8–10] its two-dimensional (2D) nature cannot provide the 3D information required for accurate quantification. Such quantification in neurobiological contexts is crucial for evaluating neuronal damage and neuroprotection, including neuronal cell counts and the extent of necrosis. Moreover, such 2D-based techniques also fail to reveal structural changes within target tissues.

Tissue clearing protocols,[11–14] in combination with deep-tissue immunolabeling [15–17] and optical sectioning microscopy techniques,[18–20] represent powerful tools for collecting 3D information at a subcellular resolution from centimeter-scale specimens. Tissue clearing techniques render biological tissues transparent by removing components that induce refraction index mismatching, which is mainly attributable to two factors, i.e., light absorption due to pigments or biological chromophores and light scattering mainly caused by lipids.[11,21] In current tissue clearing protocols, samples are fixed with 4% paraformaldehyde (PFA) for approximately 24 hours before undergoing delipidation steps that involve solvents,[22–24] aqueous solutions with denaturing reagents or detergents,[25–28] or protection with chemicals that create crosslinks to withstand harsh

electrophoretic delipidation.[29–31] Such protocols now enable imaging of whole-rodent bodies.[32,33] and even entire human organs at the cellular or subcellular level,[34] facilitating detailed and comprehensive analyses of intact biological systems. However, FFPE specimens have not reaped the benefits of these advanced techniques. For instance, although tissue clearing approaches such as CUBIC, iDISCO, CLARITY, and passive SDS treatment have been applied previously to FFPE specimens,[35–40] they have only yielded immunolabeling depths of 1-2 mm, underscoring the need for a procedure tailored to FFPE samples in order to achieve centimeter-scale tissue clearing and labeling.

Our objective was to develop a protocol capable of rendering centimeter-scale FFPE specimens optically transparent and suitable for deep immunolabeling. To this end, we took account of two critical issues. First, successful immunohistochemistry of FFPE tissue sections requires antigen retrieval to restore target conformation and expose masked epitopes.[41,42] Secondly, despite xylene treatment during paraffin processing and dewaxing protocols removing a substantial proportion of FFPE tissue lipids, certain phospholipids persist within the lipid bilayer, impeding antibody penetration and maintaining opacity.[38,43] Therefore, we aimed to devise a procedure that achieves efficient antigen retrieval and delipidation for centimeter-scale FFPE specimens. Here, we present Multiplex labeling Of Centimeter-sized Archived Tissue (MOCAT), a pipeline that employs an optimized heat-induced antigen retrieval technique to achieve that goal. We validated the effectiveness of MOCAT using FFPE human brain tissues and entire mouse brains. Using MOCAT, we demonstrate the possibility of conducting multiple rounds of immunolabeling, which allowed characterization of the same brain tissue using six different neuronal markers and revealing neuronal circuitry. We further demonstrate volumetric quantification by means of MOCAT on intact FFPE mouse brains, with statistical analysis of the FFPE samples resulting in identical trends to the results determined for fresh brains. We also showcase the broad applications of MOCAT by successfully

conducting volumetric imaging of mouse brain archived in FFPE blocks for a period of 15 years, as well as the compatibility of this apporach with expansion microscopy.

2. Results

2.1. Optimized antigen retrieval: Delipidation and epitope recovery of FFPE specimens

SDS is a detergent commonly used for lipid removal in tissue clearing methods. It is also known as an antigen retrieval agent and has been used to enhance immunolabeling signals in cells,[44] cryosections,[45] formalin-fixed human brains,[46] and epithelia of the pancreas, liver and lung.[47] Therefore, we began optimizing tissue clearing by applying two types of SDS-based approaches, passive and active, to FFPE mouse brain hemispheres and then evaluated their impacts on antigen retrieval/delipidation by means of electrophoretic immunolabeling.[15] For the passive approach, we applied a FLASH protocol published previously involving sample incubation in an SDS-based solution (4% SDS and 200 mM borate) at 54 °C for antigen retrieval and tissue clearing of epithelial cells and abdominal organs.[47] For the active approach, we employed SDS-based electrophoresis at 42 °C for 48 hours. We found that FLASH-processed samples displayed weak tyrosine hydroxylase (TH, a marker of dopaminergic neurons) signal and almost completely lacked signal of NeuN (a marker of neuronal nuclei) (Figure S1a left, 1b left, Supporting Information). We also observed that the SDS-electrophoresed sample only possessed weak TH-positive signal, as well as strong non-specific labeling (Figure S1a right, Supporting Information), with this latter considered an indicator of inadequate antigen retrieval.[48]

These results imply insufficient antigen retrieval using the SDS approaches, likely due to the low-temperature experimental conditions. In 1991, Shi et al. published a heat-induced epitope retrieval (HIER) method utilizing a temperature of 100 °C,[49] which now represents the most broad-spectrum antigen retrieval protocol for FFPE tissue sections. Superheating (i.e., temperatures

>100 °C) in pressure cookers has been reported to enhance immunohistochemistry signal intensity and stability.[50,51] However, heating with a classical antigen-retrieval citrate buffer (10 mM sodium citrate, pH 6.0) at 121 °C for 10 minutes in a pressure cooker, a condition appropriate for routine FFPE sections, only resulted in weak immunostaining signals of NeuN and SMI312 (a pan-neurofilament marker) in the middle of a 2-mm-thick FFPE mouse brain block (Figure S1b middle, Supporting Information). Since dewaxed and rehydrated FFPE specimens still have residual phospholipids that prevent antibody penetration,[38,43] we added 1% SDS into the citrate buffer to increase the delipidation capability of the HIER approach and found that NeuN and SMI312 signals were significantly enhanced (Figure S1b right, Supporting Information). However, deploying SDS at such high temperatures also resulted in tissue expansion and fragility (Figure S1b, gross view, Supporting Information), prompting us to search for a detergent condition that could achieve sufficient delipidation while retaining tissue integrity.

Accordingly, we tested four additional detergent conditions: 1% Tween 20; 1% Triton X-100; 1% sodium cholate (NaC); and 1% CHAPS. Tween 20 and Triton X-100 are commonly used to disrupt cell membranes in immunohistochemistry. NaC and CHAPS have higher critical micelle concentrations and form smaller micelles than SDS, and both have been reported as being more efficient than SDS with respect to active electrophoretic delipidation[52] and passive delipidation,[34] respectively. All tests were performed on 2-mm-thick FFPE mouse brain blocks with citrate buffer (10 mM sodium citrate, pH 6.0) at 121 °C for 10 minutes in a pressure cooker. First, we assessed amounts of residual lipids by staining with DiD (a lipophilic dye with an excitation wavelength at 649 nm). Undelipidated and SDS-delipidated (hereafter referred to as PFA-SDS) mouse brain blocks, as well as dewaxed FFPE mouse brain blocks without HIER, were also stained as controls. To prove that DiD signal quantification could be used to reflect amounts of residual lipids in tissue sections, we compared DiD signal across the FFPE group without HIER, the undelipidated group and the PFA-SDS group (**Figure 1A**, left panel). The FFPE group without HIER exhibited a higher DiD

signal intensity than the PFA-SDS group but lower than that of the undelipidated group, supporting partial lipid removal during the paraffin processing and dewaxing process. Among all of the test groups subjected to varied heated detergent conditions, only the 1% Tween 20 condition presented significantly lower lipid content compared to the FFPE without HIER group (p-value = 0.0035), achieving the same level of delipidation as the PFA-SDS group (p-value = 0.999) (Figure 1A, right panel). We also performed Oil red O staining to visualize the residual lipids and tissue morphology under bright-field microscopy (Figure S2, Supporting Information).

Next, we evaluated the efficiency of antigen retrieval by conducting immunolabeling with NeuN and SMI312 antibodies on all of the test groups and examined the signals at the center of each FFPE specimen. We found that the 1% Tween 20 group displayed the sharpest and clearest neuronal nuclei and axon bundles with a high signal-to-background ratio, indicating both successful delipidation and antigen retrieval (Figure 1B, panel 2). Interestingly, for the 1% Triton X-100, 1% NaC and 1% CHAPS groups, the fluorescence intensity of neuronal nuclei were even lower than the background signal, implying that heating these detergents might hinder nuclear epitopes (Figure 1B, panels 3, 4 and 5). We also examined the gross appearance of each group upon heating, which confirmed that the 1% Tween 20 group retained good sample integrity without apparent changes in size or color (Figure 1C). Therefore, we employed 1% Tween 20 in citrate buffer with heating in a pressure cooker at 121 °C for 10 minutes as the critical step of our MOCAT pipeline for delipidation and antigen retrieval of centimeter-scale FFPE specimens.

2.2. The MOCAT pipeline

We illustrate the complete MOCAT pipeline in Figure 1D. To retrieve a specimen from a FFPE block, the paraffin is first melted at 65-70 °C, before dewaxing at room temperature using xylene and sequentially rehydrating the tissue with alcohol. It is important to note that when working on a large sample, the dewaxing time should be increased to avoid opacity caused by residual wax due to insufficient dewaxing. Opacity can be eliminated through repeated dehydration and dewaxing steps

(Figure S3b, Supporting Information), with extended dewaxing times or repeated dewaxing steps not affecting tissue structure or antigenicity (Figure S3 and S4, Supporting Information). A typical dewaxing timeframe for paraffin sections of less than 20 µm thickness is ~20 minutes, with complete dewaxing of an entire mouse brain or similarly-sized sample achievable within 24 hours (see Materials and Methods). Optimal dewaxing times for tissue sizes between these two extremes warrant further testing.

The rehydrated FFPE samples are then treated with epoxy[31] and immersed in the optimized antigen retrieval solution (10 mM sodium citrate, 1% Tween 20, pH 6.0) at 37 °C for 24 hours, before then being heated to 121 °C for 10 minutes. The samples are then subjected to passive or active immunolabeling depending on tissue size (see Materials and Methods). After staining, the specimen is immersed in 4% PFA for 24 hours to fix the antibodies bound to epitopes, matched for the refractive index (RI), and imaged by means of lightsheet microscopy. To enable 3D phenotyping and proteomic investigations, a multi-round staining protocol involving photobleaching and classic heat-induced antigen retrieval can also be included. In this study, unless otherwise specified, all MOCAT-processed whole mouse brains had been stored in paraffin blocks for two to six months before the experiments and underwent active labeling after heating with 1% Tween 20.

To further verify MOCAT's efficacy in removing lipids from whole mouse brains, we employed coherent anti-Stokes Raman scattering (CARS), a spectroscopic technique for detecting vibrational responses of specific molecular structures (Figure 1E). In contrast to a dewaxed FFPE mouse brain (Figure 1D, left) for which we observed CARS signals from axon bundles, thus indicating the presence of myelinated lipids, both the FFPE-MOCAT-processed and PFA-SDS-treated mouse brain samples displayed significantly lower CARS signals (Figure 1E, middle and right, respectively; quantification in Figure 1F), confirming removal of myelinated lipids.

2.3. The MOCAT pipeline enables immunolabeling and registration of intact FFPE mouse brain

Previous studies have confirmed that transcriptomic and proteomic data are equally preserved in FFPE sections and fresh-frozen sections. To assess biomarker preservation within a spatial context, we investigated patterns of anti-TH antibody labeling in FFPE-MOCAT-processed mouse brains (**Figure 2**A). We observed consistent distributions of dopaminergic neurons in key tissue regions, including the striatum, nigrostriatal fiber tracts, substantia nigra, ventral tegmental area, pontine reticular nucleus, and lateral reticular nucleus, aligning with the findings of a prior study[16] (Figure 2A, left) and matching results from Allen Brain Atlas registration[53] (Figure 2A, right). Furthermore, we compared the volume of each brain region between the left and right hemispheres, which revealed minimal sample distortion (Figure 2B). Our investigation extended to a 2-mm-thick mouse brain that had been preserved in an FFPE block for 15 years. By applying MOCAT, we unveiled clear clusters of dopaminergic neurons at a cellular resolution in that specimen (Figure 2C). These results confirm the feasibility of deploying MOCAT for FFPE blocks stored long-term, even without the need for sectioning, enabling effective retrieval of information on spatial biomarkers comparable to that obtained from freshly fixed samples.

2.4. A tailored MOCAT+ pipeline enables multi-round immunolabeling of human brain tissues and whole mouse brains

Next, we investigated if MOCAT-processed whole-brain FFPE samples could be subjected to a multi-round staining process, a strategy commonly used for multiplexed immunolabeling. Chemical elution techniques utilizing detergents, reducing reagents, and denaturing reagents have been developed previously and tested on thin paraffin sections or cryosections. For thick sections, the CLARITY protocol published in 2013 involves incubation in 4% SDS solution, which was first demonstrated on a 1-mm-thick mouse hippocampus specimen. However, based on our preliminary experiments, we found that post-staining fixation is required to maintain signals in a centimeter-sized sample (i.e., a whole mouse brain) (Figure S5, Supporting Information) and the post-fixed antibodies cannot be completely stripped using SDS-based stripping protocols (Figure S6, Supporting

Information). We also observed that fixation after staining hindered subsequent rounds of staining, although this impediment could be overcome by traditional heat-induced epitope retrieval (referred to hereafter as classical HIER to avoid confusion with the aforementioned optimized antigen retrieval protocol) (Figure S7, Supporting Information). To overcome the difficulty of antibody stripping due to post-fixation, which is required for centimeter-sized specimens, we developed MOCAT+ to include a multi-round immunolabeling protocol utilizing photobleaching and classical HIER (Figure 1D). After imaging, we photobleached transparent RI-matched samples using a 100W LED white light to quench the previously labeled fluorophores. The selected duration of bleaching is dependent on sample thickness; overnight bleaching is sufficient for tissue samples of <500 μm thickness, whereas ~72 hours are required for thicker samples such as whole mouse brains (a thickness of 0.8-1 cm). Bleached specimens are then subjected to classical HIER to restore the antigenicity hindered by post-staining PFA fixation.

To explore the potential of revealing multiple neuronal circuitry in the whole FFPE mouse brain using MOCAT+, we performed a six-round immunolabeling procedure for TH, tryptophan hydroxylase 2 (TPH2), calbindin, parvalbumin (PV), choline acetyltransferase (ChAT) and SMI312, respectively, on one intact FFPE mouse brain (**Figure 3**). For each round, the brain was labeled not only with the antibody specific for the target protein, but also for lectin as a structural reference. Image datasets from each immunolabeling round were combined into a single multichannel image (**Figure 4**A), with lectin-labeled blood vessels deployed as a reference channel using Elastix,[54] demonstrating the ability of MOCAT+ to reveal the spatial distribution of different neuronal markers. We conducted a more detailed examination of the habenula-interpeduncular circuitry (Hbn-IPN circuitry) and its connection with these biomarkers. We visualized the expression of ChAT, calbindin, TH, and TPH2 in the IPN and the neighboring regions (Figure 4B). Previous studies have shown that these neurons are regulated by the Hbn-IPN circuitry through their connections with the IPN region, which plays a role in controlling emotion, addiction, and the reward process.[55,56] To demonstrate

that MOCAT+ can also be applied to human brain FFPE blocks, we performed three consecutive rounds of immunolabeling on a 1-mm-thick FFPE human brain specimen collected surgically from the temporal lobe of a brain tumor patient. For each round, the brain tissue was labeled with GFAP/lectin, SMI312/lectin, or MAP2/lectin, respectively (**Figure 5**A). Labeling homogeneity throughout the entire block was confirmed by imaging at depths of 100, 500 and 900 μm (Figure 5B).

2.5. Application of FFPE-MOCAT to mouse disease models

In disease research, volumetric imaging offers precise microenvironmental information and reveals structural changes that are essential for evaluating injuries and therapeutic effects.[13,35,57] As a first assessment of MOCAT applicability to disease models, we subjected an intact FFPE brain from an astrocytoma mouse model (see Materials and Methods) to the MOCAT pipeline to label tumor cells and astrocytes (**Figure 6**A, C). Accordingly, we could segment astrocytes surrounding the tumor (Figure 6B, D, and E) and classify them according to their distances from the tumor cells. Statistical analysis (Figure 6F) revealed that nearly half of the astrocytes were within the tumor, with 63.9% being located near the tumor surface (±200 μm). These results demonstrate that FFPE-MOCAT-derived image datasets can reveal cell distributions and the spatial architecture of disease microenvironments.

Next, we employed FFPE mouse brains from a traumatic brain injury (TBI) model to showcase the feasibility of employing MOCAT for 3D quantification of neuronal circuit recovery in disease research. Reduced dopamine levels are known to be a major cause of cognitive impairment after TBI.[58] To assess the impact on dopaminergic neural regeneration across four treatment groups (sham, sMN, aNORO@sMN, and aNORO@sMN+AMF; see Materials and Methods for details), we conducted immunolabeling using anti-TH antibodies (Figure 6G) and compared quantitative changes in the dopaminergic system among these groups. We calculated quantitative ipsilateral-to-contralateral changes for three structural features: striatum volume (Figure 6H), nigrostriatal fiber tract volume (Figure 6I), and the number of dopaminergic cells in the substantia nigra (SN) (Figure

6J). The sham group displayed a decrease (~24%) in the ratio of dopaminergic neurons on the injured side to the uninjured control side (Figure 6K), indicative of dopaminergic system malfunction or imbalance. Treatment with aNORO@sMN rescued this disease phenotype (from 76% to 94%) (Figure 6K), supporting a positive impact on dopamine production and transmission recovery post-TBI.

Next, we evaluated the therapeutic effect of aNORO@sMN on angiogenesis. To quantify angiogenesis, we selected three regions of interest around brain injury sites and segmented blood vessels (Figure 6L). The aNORO@sMN treatment group exhibited a substantial increase in blood vessel length, surface area, volume, and branch numbers (244%, 301%, 186%, and 220%, respectively) compared to the sham group (Figure 6M), indicating enhanced angiogenesis. Thus, overall, MOCAT facilitates the 3D quantification critical for assessing neuronal damage and recovery in FFPE specimens.

We also performed identical TBI procedures and 3D quantification using the SHIELD protocol and SDS-based electrophoresis for brain clearing and labeling (Figure S9, Supporting Information), which resulted in comparable quantitative outcomes compared to those determined for FFPE-MOCAT brains (Figure S10, Supporting Information). These results indicate that FFPE-MOCAT recovers biomarker signals as effectively as for freshly processed samples, even after the samples have been subjected to prolonged storage as FFPE blocks.

2.6. MOCAT enables expansion microscopy on thick FFPE samples

Expansion microscopy is a super-resolution microscopy technique that overcomes the limitations of optical diffraction by enlarging biological structures. It is achieved by synthesizing a polymer network within the specimen to anchor protein molecules, causing the specimen to physically expand and enabling analysis of sub-cellular structures.[59,60] It is generally difficult to uniformly expand heavily formaldehyde-fixed specimens, such as FFPE tissues, due to the

formaldehyde occupying the binding sites of anchoring reagents. ExPath, a modified version of protein-extension expansion microscopy (ProExM) in which the EDTA concentration in the proteinase K digestion buffer is increased, was developed to overcome this issue.[61] However, although ExPath has been successfully deployed to expand 5-μm-thick FFPE sections, it cannot uniformly expand samples beyond 1 mm even with a prolonged incubation time (**Figure 7**A). We discovered that tissues embedded in paraffin and subjected to the optimized antigen retrieval step in the MOCAT pipeline can be directly expanded using the original ProExM method without extended incubation, yielding clear staining signal for abundant targets such as SMI312 or MAP2 (Figure 7B and C).

3. Discussion

In this study, we propose MOCAT, which utilizes a heat-induced antigen retrieval protocol optimized with 1% Tween 20, to eliminate residual lipids and recover masked antigens from FFPE specimens. Our method enables labeling agents to penetrate to a depth of centimeters within such specimens, enabling large-scale neuronal circuitry analyses of archived brain tissues and providing comprehensive information that previously could not typically be obtained from conventional 3-5 μm FFPE sections. We have demonstrated herein that FFPE samples subjected to the MOCAT pipeline can be repeatedly stained without compromising their integrity. Moreover, in evaluating therapeutic efficacy for a TBI mouse model, we found that MOCAT-treated FFPE mouse brains provided as much statistical information as shortly PFA-fixed mouse brains.

3.1. MOCAT facilitates retrospective 3D analyses of neuronal diseases

FFPE processing and sectioning are standard procedures in pathology departments, and FFPE sections are routinely subjected to targeted chemical staining or immunohistochemistry for morphological observations, biomarker validations, or clinical diagnoses.[62,63] However, it is

challenging to obtain brain-wide information from conventional 3-5 μm-thick FFPE sections for studies of neurodegenerative diseases.[64] Moreover, biomarker quantifications and structural observations of 2D sections can be biased by sectioning positions and orientations. By applying MOCAT/MOCAT+, 3D histological information can be collected from FFPE specimens, thereby providing more accurate biomarker quantifications, brain-wide neuronal circuitry and cell analyses. Moreover, MOCAT/MOCAT+ may be performed on archived patient samples hosted in neuronal disease brain banks to establish a 3D biomarker atlas for neurological diseases, maximizing the utility of archived specimens. Such an atlas would represent an invaluable resource for retrospective research on biomarker distributions throughout the entire neural network, enabling tracking of their changes and interactions. The resulting comprehensive imaging datasets could also be deployed to train deep learning models, explore potential therapeutic targets, and to predict early diagnostic markers.

3.2. FFPE-MOCAT as an archival and delipidation strategy for clearing centimeter-sized tissue samples

The development of tissue clearing has revolutionized neuroscientific research. However, current tissue-clearing protocols impose a 24-hour fixation limit on mouse brains, requiring immediate tissue clearing and labeling upon animal sacrifice. MOCAT offers a solution to this predicament by enabling long-term preservation of mouse brains in FFPE blocks. Accordingly, clinical samples can be conveniently transported to imaging facilities and staining decisions can be postponed until essential analytical results, such as RNA sequencing, become available. Additionally, MOCAT minimizes excessive use of experimental mice in time-course studies by allowing brain samples in FFPE blocks after sacrifice, adhering to 3Rs principles. Consequently, researchers can decide on whole-brain staining approaches upon completing experiments, such as for toxicological or pharmacological targets, thereby avoiding the need to repeat animal experiments.

Another possible application of FFPE-MOCAT is to use it as a tissue clearing method for removing lipids. Since paraffin embedding, dewaxing, and heat-induced antigen retrieval are commonly used pathological procedures, FFPE-MOCAT can be quickly, easily, and efficiently executed in the pathology department of hospitals or research institutions, reinforcing its potential utility in clinical research.

3.3. Heating source and buffer choices for heat-induced antigen retrieval in MOCAT

Early efforts to clear and label archived FFPE specimens have only achieved limited labeling depths, [35–40] likely due to a lack of effective antigen retrieval. Protein denaturants employed in hydrophilic tissue clearing protocols, such as SDS (in CLARITY, PACT, FLASH) and urea (in CUBIC and Scale), enhance signal intensity and specificity for some types of specimens, such as cryosections or well-controlled formalin-fixed but non-paraffin-embedded tissues. However, their utility for FFPE tissues is less apparent, with temperature being considered a primary factor in their applicability in such instances.

Heat-induced antigen retrieval has been widely used since first being reported by Shi et al. in 1991, with many protocol variations since being developed, including the use of different heat sources (e.g., water baths, steamers, microwave ovens, autoclaves, and pressure cookers) and buffer choices (low molarity buffers of acid or alkaline pH).[65] Nevertheless, a unifying principle is to heat the fixed tissue sections in buffer solutions at or above 100 °C for up to 30 minutes without boiling.[51,65] In our study, we used a pressure cooker as the heat source to achieve a temperature of ~121 °C, thereby ensuring temperature stability and time efficiency. Any heating condition that is effective for FFPE sections should also work for centimeter-scale FFPE specimens (e.g., using water baths at 95-99 °C), but their effects on delipidation require further testing.

The choice of antigen retrieval solutions depends on the antibody being deployed. For example, EDTA solutions are favorable for antibodies against phosphorylated tyrosine.[65,66] Generally,

alkaline pH solutions exhibit higher antigen retrieval efficiency, but they are also more tissue-destructive and result in higher background signal compared to lower pH solutions.[41,65] In our study, we tested the addition of 1% Tween 20 to two common antigen retrieval solutions, citrate buffer (pH 6.0) and Tris-EDTA (pH 9.0), both of which yielded satisfactory staining results (Figure S10, Supporting Information), demonstrating that MOCAT facilitates the choice between acidic or alkaline antigen retrieval solutions based on antibody preference without compromising the delipidation effect.

3.4. Limitations

We acknowledge that there are some limitations to MOCAT application, which we wish to address. Firstly, the FFPE tissues we tested in this study have been limited to mouse and human brain tissues fixed under well-controlled conditions. Differences in tissue fixation procedures at different hospitals and tissue banks may affect the clarity and immunostaining efficiency of dewaxed FFPE tissues. Secondly, MOCAT has not yet been extensively tested on tissues other than the brain. Thus, its applicability and effectiveness for other tissues remain to be established. Third, the size of the samples used in this study is mostly in the range of 2-3 cm^2. Larger samples may require a prolonged incubation time and/or increased Tween 20 concentration. Fourth, endogenous fluorescence—such as GFP, YFP, and tdTomato—may be quenched during paraffin processing and thus need to be visualized by means of additional immunolabeling. Fifth, MOCAT+ may not be suitable for cases necessitating iterative staining with the same antibody. In addition, the applicability of MOCAT+ to antibodies not tested in the study requires further testing and validation. Finally, whether MOCAT-treated tissues retain sufficient molecular features and structural integrity for omics analysis warrants verification. Further research and testing will help to address these limitations and improve the applicability and effectiveness of the MOCAT pipeline we present herein.

4. Conclusions

In conclusion, as a method enabling multi-round immunolabeling of centimeter-scale archived FFPE specimens, MOCAT/MOCAT+ presents new possibilities for researching neural disease and could serve as a powerful tool for neuronal circuitry analyses and pathology. Its integration with conventional pathological procedures also renders it readily applicable in clinical settings. Through further validation across various organs and testing of its compatibility with spatial omics techniques, MOCAT could potentially catalyze broader and more comprehensive investigations in both the fundamental and clinical research domains.

5. Experimental Section

Experimental animals and human samples

We used 8-week-old CD-1 male mice to develop the MOCAT pipeline. All animal procedures and handling complied with guidelines from the Institutional Animal Care and Use Committee of Academia Sinica (IACUC protocol No.: 12-05-370), Taiwan. Information on the astrocytoma and TBI mouse models is provided in the respective subsections below. The analyses involving human participants were reviewed and approved by the Institutional Review Board of National Taiwan University Hospital (IRB No.: 202203079RINC), and all participants provided signed informed consent.

Astrocytoma animal model

All animal procedures and handling complied with guidelines from the Institutional Animal Care and Use Committee of National Tsing Hua University (IACUC protocol No.: 109067), Taiwan. ALTS1C1-GFP cells (1×10^5 cells) were implanted into the brains of 8-week-old C57BL/6 mice according to a previously published procedure.[67] In brief, 1×10^5 ALTS1C1-GFP cells were injected into the C57BL/6 mice under anesthesia at a depth of 2.5 mm and 2 mm lateral to the

midline and 1 mm posterior to the bregma. After injection, bone wax (ETHICON, W810, Somerville, NJ, USA) was applied to seal the drilled hole. Eighteen days after tumor implantation, mice were sacrificed after cardiac perfusion.

TBI mouse model

All animal procedures and handling complied with guidelines from the Institutional Animal Care and Use Committee of National Tsing Hua University (IACUC protocol Number: 110081). We divided 7-week-old C57BL/6 female mice into four groups: (1) untreated (sham), (2) treated with a paracetamol-coated silk-based microneedle (sMN), (3) treated with alternating magnetic field-responsive NO-release octahedrons (aNORO@sMN), and (4) treated with aNORO@sMN and an alternating magnetic field (aNORO@sMN+AMF). To perform traumatic brain injury (TBI), we used an electric drill to create a hole in the skull at the left motor cortex (M1 & M2) and used a 2-mm-diameter punch to cause a 1.5-mm-deep injury. For all treatments except sham, the microneedle was implanted one day post-injury to avoid excessive swelling in the injured area. For the aNORO@sMN and aNORO@sMN+AMF groups, the NO-release octahedrons (aNORO) were embedded in a silk microneedle (sMN). For the AMF-treated group, a magnetic field at a power of 3.2 kW and a frequency of 1 MHz was applied for 5 min per day until the mice were sacrificed. Additional experimental details are as described in Chan et al..[68] Mice were sacrificed 45 days after TBI induction.

Sample collection and preparation

For mouse brain samples, the mice were euthanized by injecting them with 0.2 mL of a 30% Urethane saline solution. The euthanized mice were perfused with 20 mL of cold phosphate-buffered saline (PBS) and 20 mL of 4% PFA. The collected brains were further fixed using 4% PFA at 4 °C for 24 hours. Human brain tissue specimens were surgically collected from the temporal lobe of patients and fixed with 4% PFA at 4 °C for 24 hours. For paraffin embedding, fixed specimens were

dehydrated and processed in a tissue processor (Tissue-Tek VIP 5 Jr., Sakura Finetek Japan Co. Ltd., Japan) under vacuum conditions and then embedded in paraffin wax.

SHIELD processing and SDS-electrophoretic delipidation

PFA-fixed specimens were incubated in SHIELD-OFF solution at 4 °C for 96 hours, followed by incubation for 24 hours in SHIELD-ON solution at 37 °C. All reagents were prepared using SHIELD kits (LifeCanvas Technologies, Seoul, South Korea) according to the manufacturer's instructions. For SDS-electrophoretic delipidation, SHIELD-processed specimens were placed in a stochastic electro-transport machine (SmartClear Pro II, LifeCanvas Technologies, Seoul, South Korea) running at a constant current of 1.2 A for 5-7 days. The delipidated specimens were washed with PBST at room temperature for at least 1 day.

Evaluating the extent of delipidation

Mouse brain slices (2-mm thick) of various treatment conditions were cut into 20-µm-thick cryosections for subsequent DiD or Oil red O staining. For DiD staining, cryosections were post-fixed with 4% PFA at room temperature for 5 minutes. The sections were then rinsed with distilled water and immersed in PBST (PBS with 0.1% Triton X-100) for 10 minutes to remove OCT. These sections were stained with 0.0025 uM DiD/PBST solution at room temperature for 1 hour, before rinsing them with distilled water and washing with 1% SDS for several seconds to remove excess DiD. The slides were mounted in 50% glycerol and imaged under a Zeiss 780 confocal microscope using a 10× 0.75NA Plan-Apochromat objective (Zeiss). For Oil red O staining, the sections were post-fixed with a 4% formal-calcium solution for 5 minutes and then rinsed with distilled water. The fixed sections were pre-incubated in 60% isopropanol for 5 minutes and then stained with fresh Oil red O working solution (0.3% Oil red O in 60% isopropanol) for 15 minutes. The sections were briefly washed with 60% isopropanol and mounted in glycerine jelly. Images were acquired using a 3DHISTECH Pannoramic 250 slide scanner with a 40× 0.95NA Plan-Apochromat objective (Zeiss). Details of statistical analyses are described in the *Quantification and Statistics* section below.

Comparison of brain region volume

Autofluorescence-channel imaging datasets of whole mouse brains were aligned to the BrainGlobe Atlas API[53] using the aMAP tool.[69] The volume of each brain subregion was then obtained and organized based on anatomical hierarchy using the Allen Brain Atlas. The 679 subregions were merged into 78 brain regions at the same anatomical hierarchy as the hippocampus. The brain region volume of right and left hemisphere of the FFPE-MOCAT mouse brain was compared and plotted using GraphPad Prism 9.5.1 (GraphPad Software Inc., San Diego, CA, USA).

MOCAT pipeline

The MOCAT pipeline is illustrated in Figure 1C and described in detail below.

Deparaffination and rehydration. FFPE blocks were incubated at 65-70 °C to melt the paraffin. Residual paraffin was removed through immersion in xylene for 24 hours, with the xylene being changed at least twice. Dewaxed brains were rehydrated with 100%, 100%, 95%, 85%, 75%, and 55% alcohol diluted with distilled water. The rehydrated brains were then washed with PBS.

Optimized antigen retrieval. Specimens were incubated overnight at 37 °C in a modified citrate buffer (10 mM sodium citrate, 1% Tween 20, pH 6.0). The specimens and buffer were then heated for 10 minutes at 121 °C in a pressure cooker (Bio SB, Santa Barbara, CA, USA) and kept in the pressure cooker until the temperature dropped below 100 °C (for approximately 15 minutes). Next, the specimens were removed from the cooker and cooled for 10 minutes at room temperature. The specimens were then washed three times in PBST, with each wash lasting 1 hour.

Electrophoretic immunolabeling (active staining). The procedure was modified from the previously published eFLASH protocol[15] and was conducted in a SmartLabel System (LifeCanvas Technologies, Seoul, South Korea). The specimens were preincubated overnight at room temperature in sample buffer (240 mM Tris, 160 mM CAPS, 20% w/v D-sorbitol, 0.9% w/v sodium deoxycholate). Each preincubated specimen was placed in a sample cup (provided by the manufacturer with the SmartLabel System) containing primary and corresponding secondary

antibodies diluted in 8 mL of sample buffer. Information on antibodies and their optimized quantities is detailed in Supplementary Table 1. The specimens in the sample cup and 500 mL of labeling buffer (240 mM Tris, 160 mM CAPS, 20% w/v D-sorbitol, 0.2% w/v sodium deoxycholate) were loaded into the SmartLabel System. The device was operated at a constant voltage of 90 V with a current limit of 400 mA. After 18 hours of electrophoresis, 300 mL of booster solution (20% w/v D-sorbitol, 60 mM boric acid) was added, and electrophoresis continued for 4 hours. Labeled specimens were washed twice (3 hours per wash) with PTwH (1× PBS with 0.2% w/v Tween-20 and 10 μg/mL heparin),[23] and then post-fixed with 4% PFA at room temperature for 1 day. Post-fixed specimens were washed twice (3 hours per wash) with PBST to remove any residual PFA.

Refractive index (RI) matching. Before imaging, the specimens were RI-matched by immersing them in NFC1 and NFC2 solutions (Nebulum, Taipei, Taiwan) at room temperature for 1 day for each solution.

Volumetric imaging and 3D visualization. For centimeter-scale specimens, images were acquired using a light-sheet microscope (SmartSPIM, LifeCanvas Technologies, Seoul, South Korea) with a 4x customized immersion objective. For samples <3 mm thick, imaging was performed using a multipoint confocal microscope (Andor Dragonfly 200, Oxford Instruments, UK). 3D visualization was performed using Imaris software (Imaris 9.5.0, Bitplane, Belfast, UK).

Photobleaching. Immunolabeled and imaged specimens were placed in a multi-well plate and immersed in RI-matching solutions so they retained transparency. The plate was then sealed with paraffin. A 100-W projection lamp with an LED array was placed on the plate to quench fluorescence signals. A representative photobleaching apparatus constructed using off-the-shelf components is shown in Supplementary Figure 11. In our experience, approximately 18 hours photobleaching is sufficient for a 2-mm-thick sample, whereas 3 days is required for a whole mouse brain (approximately 8 mm to 1 cm in thickness).

Raman microscopy

A Yb:KGW laser (Carbide, Light Conversion) emitting a 190 fs, 200 kHz, 20 W pulse train at a 1030 nm wavelength was used to generate a supercontinuum via a double-pass multiple-plate continuum module. The resulting spectrum (600-1300 nm) was spectrally sliced by tunable color filters (3G LVLWP, LVSWP, and LVFBP, Delta) to provide pump (725 nm) and Stokes (914 nm) beams, which could address the Raman shift (2850 cm-1) of lipids. The two beams were temporally and spatially overlapped, and then guided into a commercial upright microscope (Axio Examiner.Z1, Zeiss) with a scanning unit (LSM7MP, Zeiss) to achieve raster scanning on the x-y plane. A single 20x water immersion objective (UMPLFLN 20XW, Olympus) was used to focus the combined laser beams on the mouse sample. Epi-CARS signal at 601 nm was spectrally separated from the incident radiation with a bandpass filter (BP 565-610, Zeiss) and detected using a photomultiplier tube.

Multichannel image registration

For six-round immunolabeling of a single whole mouse brain, each dataset included one structural reference channel stained with lectin and one antibody-stained channel. The first round of staining served as the standard brain, with lectin channel images of each subsequent dataset being registered to the lectin channel of the standard brain using the Elastix toolbox.[54] The transformation parameters obtained from rigid and B-spline deformable registration of the lectin channels were then applied to the antibody-stained channels. The transformed images were merged and visualized using Imaris software. In the case of three-round immunolabeling of human specimens, the image datasets from the three rounds were registered and resampled using Amira software (Thermo Fisher Scientific, Waltham, MA, USA), and then merged and visualized using Imaris software.

Expansion microscopy and ExPath

Expansion microscopy was performed using the proExM protocol.[58] A 1-mm-thick MOCAT-processed FFPE mouse brain slice was incubated in anchoring solution (0.01% w/v methacrylic acid N-hydroxysuccinimide ester in 1×PBS) at 4 °C for 24 hours. After anchoring, the sample was washed twice (5 minutes each time) with PBS at room temperature and then rinsed twice (5 minutes

each time) in acrylamide monomer solution (2 M NaCl, 8.625% w/w sodium acrylate, 2.5% w/w acrylamide, 0.15% w/w N,N'-methylene-bisacrylamide in 1×PBS) at 4 °C. For gelation, the specimen was pre-incubated in gelation solution (0.02% w/w ammonium persulfate (APS), 0.02% w/w tetramethyl-ethylenediamine (TEMED), and 0.01% w/w 4-hydroxy-2,2,6,6-tetramethylpiperidin-1-oxyl (4-hydroxy-TEMPO) in monomer solution) for 5 minutes at 4 °C, and then moved into fresh gelation solution for an additional 25 minutes. The specimen in gelation solution was then transferred to a humidified 37 °C incubator for 2 hours. The gel was then immersed in a digestion solution (8 units/ml proteinase K, 50 mM Tris, 1 mM EDTA, 0.5% w/v Triton X-100, 1M NaCl, pH 8.0) at 37 °C for 4 hours. After digestion, the gel was immersed in an excess of deionized water for 0.5-2 hours to expand. This step was repeated 3−5 times with fresh water until the size of the sample ceased to increase.

For the ExPath experiment, a 1-mm-thick FFPE mouse slice was dewaxed, rehydrated and underwent the same anchoring and gelation steps as described above. The gel was digested in ExPath digestion solution (8 units/ml proteinase K, 50 mM Tris, 25 mM EDTA, 0.5% w/v Triton X-100, 0.8M NaCl, pH 8.0) at 60 °C for 3 hours.[59]

Post-expansion immunolabeling

Digested gels were washed twice (20 minutes each time) in PBS, and then incubated in a primary antibody cocktail containing anti-SMI312 (Biolegend, 837904, 1:500 dilution), anti-MAP2 (Cell Signaling Technology, #8707, 1:500 dilution), 2% v/v normal goat serum (Jackson ImmunoResearch, 005-000-121, 1:500 dilution), and 0.1% w/v Triton X-100 in 1×PBS at 4 °C for 24 hours. The gels were then washed three times (20 minutes each time) in wash buffer (30 mM sodium chloride, 0.1% w/v Triton X-100 in 1×PBS) and incubated in a secondary antibody cocktail containing Alexa Fluor® 647 AffiniPure goat anti-mouse IgG (Jackson ImmunoResearch, 115-605-003, 1:500 dilution), Rhodamine Red™-X (RRX) AffiniPure goat anti-rabbit IgG (Jackson ImmunoResearch, 111-295-003, 1:500 dilution), 0.2% v/v normal goat serum, and 0.1% w/v Triton X-100 in 1×PBS at 4 °C for

24 hours. The antibody-labeled gels were washed three times (20 minutes each time) in wash buffer and then placed in deionized water for expansion. For nuclei staining, propidium iodine was added to deionized water at a final concentration of 1 μg/ml during expansion.

Quantification and statistics

To quantify the extent of delipidation (Figure 1A), DiD-stained sections were imaged at an excitation wavelength of 642 nm. To quantify the fluorescence intensity, 10 regions of interest (ROI) of 0.8 × 0.8 mm were selected randomly within the cortex of each specimen. The gray (pixel) value of each ROI was measured using Fiji,[70] Mean values and standard deviations (SD) were plotted using GraphPad Prism 9.5.1 (GraphPad Software Inc., San Diego, CA, USA). The significance of the difference in mean values was determined by means of one-way ANOVA with Tukey's multiple comparison tests at an α level = 0.05 (*$P < 0.05$; **$P < 0.01$; ***$P < 0.001$; ****$P < 0.0001$).

For the Raman signal quantification shown in Figure 1F, gray values of 18 Raman images (0.4 × 0.4 mm) at a different depth for each group were measured using Fiji. The mean values and SD were determined, and the significance of differences were also calculated by means of one-way ANOVA using GraphPad Prism as described above.

For the astrocyte-tumor distance analysis shown in Figure 6F, the astrocytes were segmented using the SPOT module of Imaris based on a fluorecence intensity threshold and point spread function (PSF) size definition. GFP-expressing tumors were segmented using the Surface module of Imaris. Distances of all segments were calculated in Imaris.

To quantify dopaminergic regions in TBI mouse brains, the volume of the striatum and nigrostriatal fiber tracts was calculated using the Surface module of Imaris, and cell number in the substantia nigra was determined using the SPOT module. To demonstrate the similarity of quantification results from FFPE-MOCAT and PFA-SDS brains, the quantification data for the injured side of each brain was normalized according to the results for the corresponding contralateral side. Mean values and SD were plotted using GraphPad Prism (N = 3 in Figure 6K and Supplementary Figure 9a). The

significance of the difference in mean values was determined by means of one-way ANOVA with Tukey's multiple comparison tests at an α level = 0.05 (*P < 0.05; **P < 0.01; ***P < 0.001; ****P < 0.0001).

To evaluate angiogenesis, we selected three ROIs (each of 0.6 × 0.6 × 0.6 mm) close to the injury site. The Surface module of Imaris was used to segment the blood vessels and calculate their total volume and surface area. Their length and numbers of bifurcation points were calculated using Vessap.[71] Erosion and dilation were performed to remove false-negative pixels and to avoid false centerline detections. Next, the centerlines were extracted by means of a 3D thinning algorithm.[72] The bifurcation points were detected using the surrounding pixels of each point to define a point that splits into two or more vessels. Mean values, SD, and the significance of differences were calculated by independent *t* test using GraphPad Prism.

Supporting Information

Supporting Information is available from the Wiley Online Library or from the author.

Acknowledgements

We thank the Brain Research Center, National Tsing-Hua University, Taiwan and Pathology core, Institute of Biomedical Sciences, Academia Sinica, Taiwan for the technical assistance. This work was funded by the grants from National Science and Technology Council (NSTC-111-2636-B-007-007, NSTC-07-2314-B-007-003-MY3, NSTC-111-2321-B-002-016, MOST-110-2321-B-010-006). This work was also supported by the Brain Research Center under the Higher Education Sprout Project, co-funded by the Ministry of Education and the National Science and Technology Council in Taiwan.

Conflict of Interest

The authors declare no conflict of interest.

Data Availability Statement

The data that support the findings of this study are available within the article and its supporting information.

References

1. Rajput, A. H. & Rajput, A. Saskatchewan Movement Disorders Program. *Can. J. Neurol. Sci.* **42**, 74–87 (2015).

2. Hernandez-Ronquillo, L. *et al.* The Concept of an Epilepsy Brain Bank. *Front. Neurol.* **11**, 553157 (2020).

3. Latimer, C. S. *et al.* Protocol for the Systematic Fixation, Circuit-Based Sampling, and Qualitative and Quantitative Neuropathological Analysis of Human Brain Tissue. *Methods Mol. Biol.* **2561**, 3–30 (2023).

4. Talari, K. & Goyal, M. Retrospective Studies – Utility and Caveats. *https://doi.org/10.4997/jrcpe.2020.409* **50**, 398–402 (2020).

5. Jacobsen, S. B., Tfelt-Hansen, J., Smerup, M. H., Andersen, J. D. & Morling, N. Comparison of whole transcriptome sequencing of fresh, frozen, and formalin-fixed, paraffin-embedded cardiac tissue. *PLoS One* **18**, e0283159 (2023).

6. Zhao, L. *et al.* FACT-seq: profiling histone modifications in formalin-fixed paraffin-embedded samples with low cell numbers. *Nucleic Acids Res.* **49**, e125–e125 (2021).

7. Zhong, J. *et al.* Enhanced and controlled chromatin extraction from FFPE tissues and the application to ChIP-seq. *BMC Genomics* **20**, 1–11 (2019).

8. Fraggetta, F. *et al.* The Importance of eSlide Macro Images for Primary Diagnosis with Whole Slide Imaging. *J. Pathol. Inform.* **9**, 46–46 (2018).

9. Kumar, N., Gupta, R. & Gupta, S. Whole Slide Imaging (WSI) in Pathology: Current Perspectives and Future Directions. *J. Digit. Imaging* **33**, 1034–1040 (2020).

10. Patel, A. *et al.* Contemporary Whole Slide Imaging Devices and Their Applications within the Modern Pathology Department: A Selected Hardware Review. *J. Pathol. Inform.* **12**, 50 (2021).

11. Richardson, D. S. & Lichtman, J. W. Clarifying Tissue Clearing. *Cell* **162**, 246–257 (2015).

12. Ueda, H. R. *et al.* Tissue clearing and its applications in neuroscience. *Nature Reviews Neuroscience* vol. 21 61–79 (2020).

13. Gómez-Gaviro, M. V., Sanderson, D., Ripoll, J. & Desco, M. Biomedical applications of tissue clearing and three-dimensional imaging in health and disease. *iScience* **23**, 101432 (2020).

14. Richardson, D. S. *et al.* TISSUE CLEARING. *Nat. Rev. Methods Prim.* **1**, (2021).

15. Yun, D. H. *et al.* Ultrafast immunostaining of organ-scale tissues for scalable proteomic phenotyping. *bioRxiv* 660373 (2019) doi:10.1101/660373.

16. Susaki, E. A. *et al.* Versatile whole-organ/body staining and imaging based on electrolyte-gel properties of biological tissues. *Nat. Commun. 2020 111* **11**, 1–22 (2020).

17. Yau, C. N. *et al.* Principles of deep immunohistochemistry for 3D histology. (2023) doi:10.1016/j.crmeth.2023.100458.

18. Conchello, J. A. & Lichtman, J. W. Optical sectioning microscopy. *Nat. Methods 2005 212* **2**, 920–931 (2005).

19. Dodt, H. U. *et al.* Ultramicroscopy: Three-dimensional visualization of neuronal networks in the whole mouse brain. *Nat. Methods* **4**, 331–336 (2007).

20. Reynaud, E. G., Kržič, U., Greger, K. & Stelzer, E. H. K. Light sheet-based fluorescence microscopy: More dimensions, more photons, and less photodamage. *HFSP J.* **2**, 266–275 (2008).

21. Yu, T., Zhu, J., Li, D. & Zhu, D. Physical and chemical mechanisms of tissue optical clearing. *iScience* **24**, 102178 (2021).

22. Ertürk, A. *et al.* Three-dimensional imaging of solvent-cleared organs using 3DISCO. *Nat. Protoc.* **7**, 1983–1995 (2012).

23. Renier, N. *et al.* IDISCO: A simple, rapid method to immunolabel large tissue samples for volume imaging. *Cell* **159**, 896–910 (2014).

24. Jing, D. *et al.* Tissue clearing of both hard and soft tissue organs with the pegasos method. *Cell Res*. **28**, 803–818 (2018).

25. Hama, H. *et al.* Scale: a chemical approach for fluorescence imaging and reconstruction of transparent mouse brain. *Nat. Neurosci. 2011 1411* **14**, 1481–1488 (2011).

26. Susaki, E. A. *et al.* Whole-brain imaging with single-cell resolution using chemical cocktails and computational analysis. *Cell* **157**, 726–739 (2014).

27. Hama, H. *et al.* ScaleS: An optical clearing palette for biological imaging. *Nat. Neurosci.* **18**, 1518–1529 (2015).

28. Tainaka, K. *et al.* Chemical Landscape for Tissue Clearing Based on Hydrophilic Reagents. *Cell Rep.* **24**, 2196-2210.e9 (2018).

29. Chung, K. *et al.* Structural and molecular interrogation of intact biological systems. *Nature* **497**, 332–337 (2013).

30. Murray, E. *et al.* Simple, Scalable Proteomic Imaging for High-Dimensional Profiling of Intact Systems. *Cell* **163**, 1500–1514 (2015).

31. Park, Y.-G. *et al.* Protection of tissue physicochemical properties using polyfunctional crosslinkers. *Nat. Biotechnol.* **37**, 73–83 (2019).

32. Cai, R. *et al.* Panoptic imaging of transparent mice reveals whole-body neuronal projections and skull–meninges connections. *Nat. Neurosci.* **22**, 317–327 (2019).

33. Mai, H. *et al.* Whole-body cellular mapping in mouse using standard IgG antibodies. *Nat. Biotechnol. 2023* 1–11 (2023) doi:10.1038/s41587-023-01846-0.

34. Zhao, S. *et al.* Cellular and Molecular Probing of Intact Human Organs. *Cell* **180**, 796-812.e19 (2020).

35. Chen, Y. *et al.* Three-dimensional imaging and quantitative analysis in CLARITY processed breast cancer tissues. *Sci. Rep.* **9**, 1–13 (2019).

36. Hughes, C., Gaunt, L., Brown, M., Clarke, N. W. & Gardner, P. Assessment of paraffin removal from prostate FFPE sections using transmission mode FTIR-FPA imaging. *Anal. Methods* **6**, 1028–1035 (2014).

37. Lai, H. M. *et al.* Next generation histology methods for three-dimensional imaging of fresh and archival human brain tissues. *Nat. Commun. 2018 91* **9**, 1–12 (2018).

38. Nojima, S. *et al.* CUBIC pathology: Three-dimensional imaging for pathological diagnosis. *Sci. Rep.* **7**, 1–14 (2017).

39. Tanaka, N. *et al.* Whole-tissue biopsy phenotyping of three-dimensional tumours reveals patterns of cancer heterogeneity. *Nat. Biomed. Eng.* **1**, 796–806 (2017).

40. Tanaka, N. *et al.* Mapping of the three-dimensional lymphatic microvasculature in bladder tumours using light-sheet microscopy. *Br. J. Cancer 2018 1187* **118**, 995–999 (2018).

41. Shi, S.-R., Cote, R. J. & Taylor, C. R. Antigen Retrieval Techniques: Current Perspectives. *J. Histochem. Cytochem.* **49**, 931–937 (2001).

42. Thavarajah, R., Mudimbaimannar, V. K., Elizabeth, J., Rao, U. K. & Ranganathan, K. Chemical and physical basics of routine formaldehyde fixation. *J. Oral Maxillofac. Pathol.* **16**, 400 (2012).

43. Denti, V. *et al.* Antigen Retrieval and Its Effect on the MALDI-MSI of Lipids in Formalin-Fixed Paraffin-Embedded Tissue. *J. Am. Soc. Mass Spectrom.* **31**, 1619–1624 (2020).

44. Robinson, J. M. & Vandré, D. D. Antigen retrieval in cells and tissues: Enhancement with sodium dodecyl sulfate. *Histochem. Cell Biol.* **116**, 119–130 (2001).

45. Brown, D. *et al.* Antigen retrieval in cryostat tissue sections and cultured cells by treatment with sodium dodecyl sulfate (SDS). *Histochem. Cell Biol.* **105**, 261–267 (1996).

46. Woelfle, S. *et al.* CLARITY increases sensitivity and specificity of fluorescence immunostaining in long-term archived human brain tissue. *BMC Biol.* **21**, 1–28 (2023).

47. Messal, H. A. *et al.* Antigen retrieval and clearing for whole-organ immunofluorescence by FLASH. *Nat. Protoc.* **16**, 239–262 (2021).

48. Kim, S. W., Roh, J. & Park, C. S. Immunohistochemistry for Pathologists: Protocols, Pitfalls, and Tips. *J. Pathol. Transl. Med.* **50**, 411 (2016).

49. Shi, S. R., Key, M. E. & Kalra, K. L. Antigen retrieval in formalin-fixed, paraffin-embedded tissues: an enhancement method for immunohistochemical staining based on microwave oven heating of tissue sections. *J. Histochem. Cytochem.* **39**, 741–748 (1991).

50. Norton, A. J., Jordan, S. & Yeomans, P. Brief, high-temperature heat denaturation (pressure cooking): A simple and effective method of antigen retrieval for routinely processed tissues. *J. Pathol.* **173**, 371–379 (1994).

51. Taylor, C. R. *et al.* Comparative study of antigen retrieval heating methods: microwave, microwave and pressure cooker, autoclave, and steamer. *Biotech. Histochem.* **71**, 263–270 (1996).

52. Na, M. *et al.* Sodium Cholate-Based Active Delipidation for Rapid and Efficient Clearing and Immunostaining of Deep Biological Samples. *Small Methods* **6**, (2022).

53. Claudi, F. *et al.* BrainGlobe Atlas API: a common interface for neuroanatomical atlases. *J. Open Source Softw.* **5**, 2668 (2020).

54. Klein, S., Staring, M., Murphy, K., Viergever, M. A. & Pluim, J. P. W. elastix: a toolbox for intensity-based medical image registration. *IEEE Trans. Med. Imaging* **29**, 196–205 (2010).

55. McLaughlin, I., Dani, J. A. & DeBiasi, M. The medial habenula and interpeduncular nucleus circuitry is critical in addiction, anxiety, and mood regulation. *J. Neurochem.* **142**, 130–143 (2017).

56. Fakhoury, M. The dorsal diencephalic conduction system in reward processing: Spotlight on the anatomy and functions of the habenular complex. *Behav. Brain Res.* **348**, 115–126 (2018).

57. Liebmann, T. *et al.* Three-Dimensional Study of Alzheimer's Disease Hallmarks Using the iDISCO Clearing Method. *Cell Rep.* **16**, 1138–1152 (2016).

58. Jenkins, P. O. *et al.* Dopaminergic abnormalities following traumatic brain injury. *Brain* **141**, 797–810 (2018).

59. Chen, F., Tillberg, P. W. & Boyden, E. S. Expansion microscopy. *Science (80-.).* **347**, 543–548 (2015).

60. Tillberg, P. W. *et al.* Protein-retention expansion microscopy of cells and tissues labeled using standard fluorescent proteins and antibodies. *Nat. Biotechnol.* **34**, 987–992 (2016).

61. Zhao, Y. *et al.* Nanoscale imaging of clinical specimens using pathology-optimized expansion microscopy. *Nat. Biotechnol. 2017 358* **35**, 757–764 (2017).

62. Berg, D., Malinowsky, K., Reischauer, B., Wolff, C. & Becker, K. F. Use of formalin-fixed and paraffin-embedded tissues for diagnosis and therapy in routine clinical settings. *Methods Mol. Biol.* **785**, 109–122 (2011).

63. Steeghs, E. M. P. *et al.* Comprehensive routine diagnostic screening to identify predictive mutations, gene amplifications, and microsatellite instability in FFPE tumor material. *BMC Cancer* **20**, 1–15 (2020).

64. Golub, V. M. *et al.* Neurostereology protocol for unbiased quantification of neuronal injury and neurodegeneration. *Front. Aging Neurosci.* **7**, 158767 (2015).

65. Krenacs, L., Krenacs, T., Stelkovics, E. & Raffeld, M. Heat-Induced Antigen Retrieval for Immunohistochemical Reactions in Routinely Processed Paraffin Sections. *Methods Mol. Biol.* **588**, 103 (2010).

66. Pileri, S. A. *et al.* Antigen retrieval techniques in immunohistochemistry: comparison of different methods. *J. Pathol* **183**, 116–123 (1997).

67. Wang, S. C., Hong, J. H., Hsueh, C. & Chiang, C. S. Tumor-secreted SDF-1 promotes glioma invasiveness and TAM tropism toward hypoxia in a murine astrocytoma model. *Lab. Invest.* **92**, 151–162 (2012).

68. Chan, Y. C. *et al.* In situ magnetoelectric generation of nitric oxide and electric stimulus for nerve therapy by wireless chargeable molybdenum carbide octahedrons. *Nano Today* **51**, 101935 (2023).

69. Niedworok, C. J. *et al.* aMAP is a validated pipeline for registration and segmentation of high-resolution mouse brain data. *Nat. Commun. 2016 71* **7**, 1–9 (2016).

70. Schindelin, J. *et al.* Fiji: an open-source platform for biological-image analysis. *Nat. Methods 2012 97* **9**, 676–682 (2012).

71. Todorov, M. I. *et al.* Machine learning analysis of whole mouse brain vasculature. *Nat. Methods 2020 174* **17**, 442–449 (2020).

72. Lee, T. C., Kashyap, R. L. & Chu, C. N. Building Skeleton Models via 3-D Medial Surface Axis Thinning Algorithms. *CVGIP Graph. Model. Image Process.* **56**, 462–478 (1994).

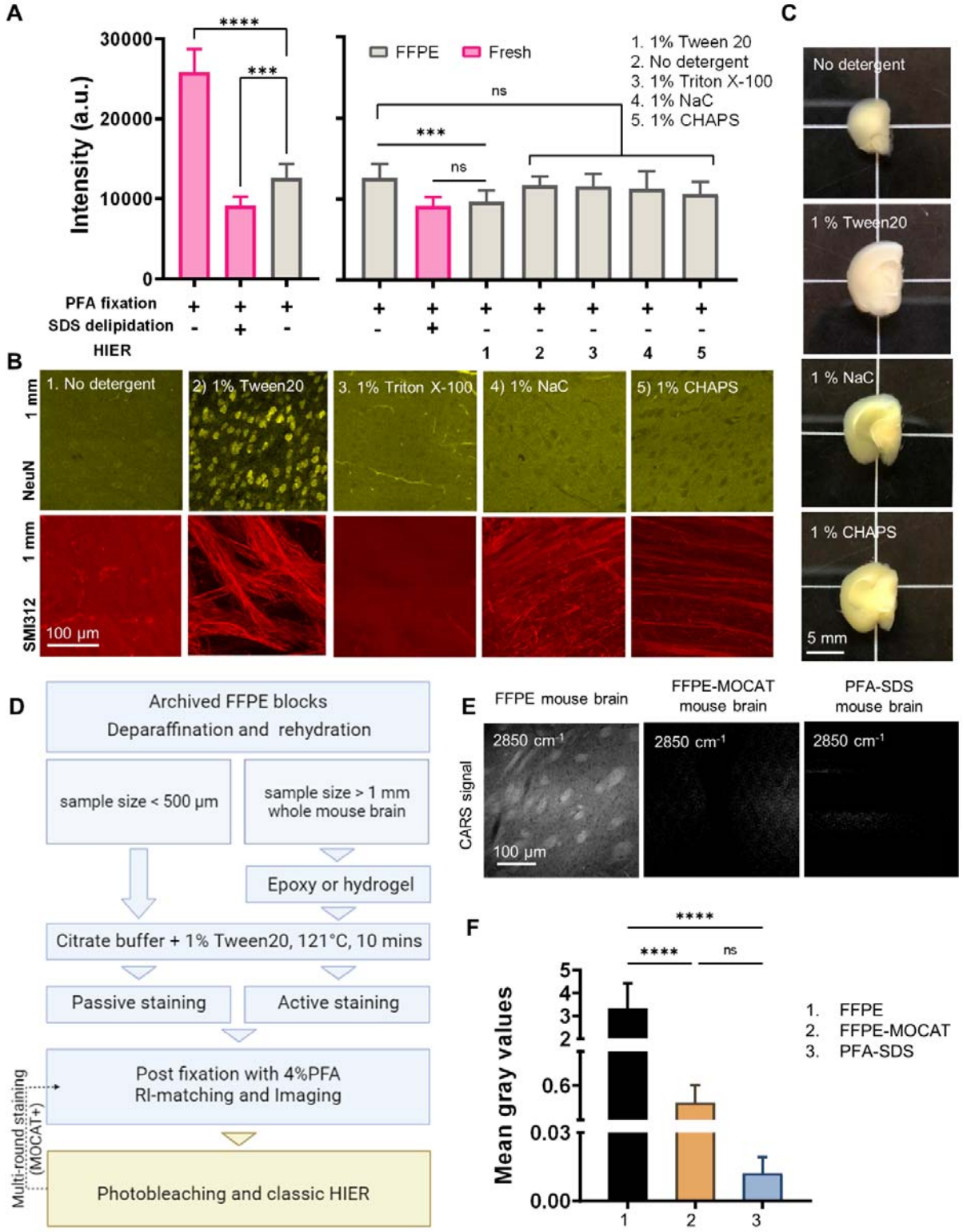
A
Intensity (a.u.)
30000
20000
10000
0
****
***
FFPE
Fresh
1. 1% Tween 20
2. No detergent
3. 1% Triton X-100
4. 1% NaC
5. 1% CHAPS
ns
***
ns
PFA fixation
SDS delipidation
HIER
1
2
3
4
5
B
1. No detergent
2) 1% Tween20
3. 1% Triton X-100
4) 1% NaC
5) 1% CHAPS
1 mm
NeuN
1 mm
SMI312
100 µm
C
No detergent
1 % Tween20
1 % NaC
1 % CHAPS
5 mm
D
Archived FFPE blocks
Deparaffination and rehydration
sample size < 500 µm
sample size > 1 mm
whole mouse brain
Epoxy or hydrogel
Citrate buffer + 1% Tween20, 121°C, 10 mins
Passive staining
Active staining
Post fixation with 4%PFA
RI-matching and Imaging
Multi-round staining
(MOCAT+)
Photobleaching and classic HIER
E
FFPE mouse brain
FFPE-MOCAT
mouse brain
PFA-SDS
mouse brain
CARS signal
2850 cm-1
2850 cm-1
2850 cm-1
100 µm
F
Mean gray values
5
4
3
2
0.6
0.03
0.00
****
****
ns
1. FFPE
2. FFPE-MOCAT
3. PFA-SDS
1
2
3

Figure 1. Development of the MOCAT pipeline.
(**A**) Comparison of DiD signal intensity in 2-mm-thick slices of undelipidated formaldehyde-fixed mouse brain, PFA-SDS mouse brain, and FFPE mouse brain treated under various detergent conditions.
(**B**) Multi-point confocal fluorescence images of neuronal nuclei in the cortex (top row) and axons in the striatum (bottom row) from 2-mm-thick FFPE mouse brain slices that had been treated under various detergent conditions. Images of optical sections captured at a depth of 1 mm are shown. Detergent types and concentrations are indicated. NeuN, a neuronal nuclear marker; SMI312, a pan-axonal marker.
(**C**) Gross views of 2-mm-thick slices of FFPE mouse brain treated under various detergent conditions.
(**D**) Schematic of the MOCAT pipeline.
(**E**) Images of coherent anti-Stokes Raman scattering (CARS) of dewaxed FFPE mouse brain, MOCAT-processed FFPE mouse brain, and PFA-SDS mouse brain. The images were taken at a Raman shift of 2850 cm^{-1} to address the CH2 vibration frequency.
(**F**) Statistical analysis of the gray values for the three treatment groups in (E). Gray values for 18 z-continuous images of each group were analyzed.
Statistical analysis: (A) n = 10; (E) n = 18. Mean ± SD, * $p < 0.05$, ** $p < 0.01$, *** $p < 0.001$, **** $p < 0.0001$, one-way ANOVA with Tukey's multiple comparison test.

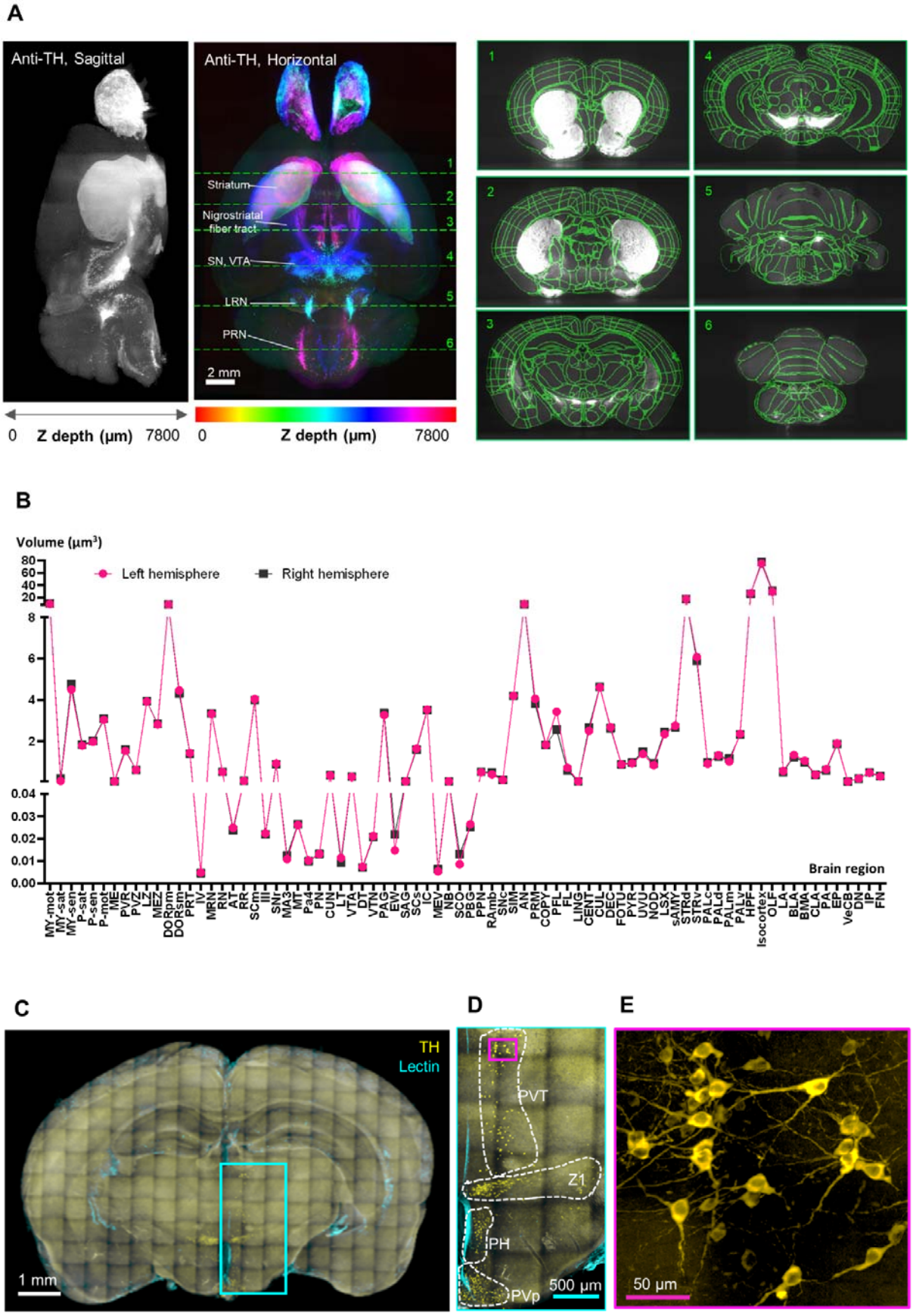
A
Anti-TH, Sagittal
Anti-TH, Horizontal
Striatum
Nigrostriatal fiber tract
SN, VTA
LRN
PRN
2 mm
0 Z depth (μm) 7800
0 Z depth (μm) 7800
B
Volume (μm³)
Left hemisphere
Right hemisphere
Brain region
C
TH
Lectin
1 mm
D
PVT
Z1
PH
PVp
500 μm
E
50 μm

Figure 2. Validation of the MOCAT pipeline.
(**A**) Brain-wide tyrosine hydroxylase (TH) expression (left panel) and registration (right panel) in FFPE-MOCAT C57BL/6 mouse brains. Whole mouse brain images were acquired using light-sheet microscopy, and the 3D-rendered images of the horizontal (XY) and sagittal (YZ) views are shown. Major dopaminergic regions are indicated: SN (substantia nigra), VTA (ventral tegmental area), LRN (lateral reticular nucleus), and PRN (pontine reticular nucleus). The results of brain registration for these regions (marked with green dotted lines and numbered in the XY view) are displayed from the coronal (XZ) view in the right panel.
(**B**) Comparison of brain region volumes between the left and right hemispheres of an FFPE-MOCAT mouse brain. All abbreviations are listed in Supplementary Table 2.
(**C** to **E**) Application of MOCAT to a 15-year-old FFPE block with TH-immunolabeling and multi-point confocal imaging. Specimen thickness: 2 mm.
(**C**) The projection image.
(**D**) Magnification of the cyan-lined region in (C). Dopaminergic regions are indicated. PVT, paraventricular nucleus of thalamus; PH, posterior hypothalamic nucleus; PVp, periventricular hypothalamic nucleus.
(**E**) Magnification of the magenta-lined region in (D). Scale bars are indicated in each panel.

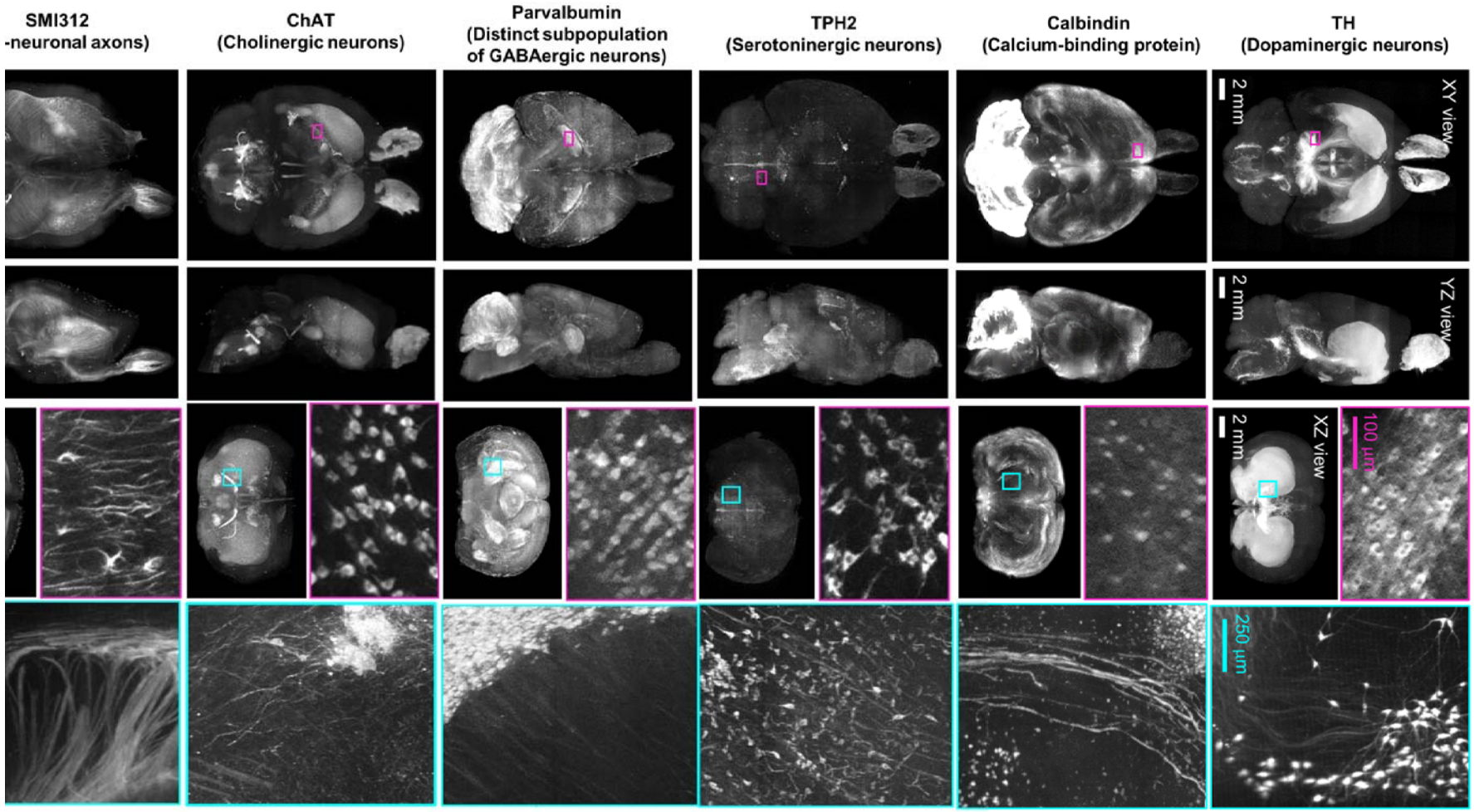
SMI312
-neuronal axons)
ChAT
(Cholinergic neurons)
Parvalbumin
(Distinct subpopulation
of GABAergic neurons)
TPH2
(Serotoninergic neurons)
Calbindin
(Calcium-binding protein)
TH
(Dopaminergic neurons)
XY view
YZ view
XZ view
2 mm
100 µm
250 µm

Figure 3. Multi-round immunostaining of FFPE-MOCAT whole mouse brain (MOCAT+). Light-sheet microscopy imaging datasets of six-round immunolabeling performed on one whole FFPE mouse brain. Projection images of the horizontal (XY), sagittal (YZ), and transverse (XZ) views are shown. Projection images (200-μm thick) of magenta-lined and cyan-lined regions marked in the XY and XZ views are magnified and displayed within correspondingly colored frames. Scale bars are indicated in the first row.

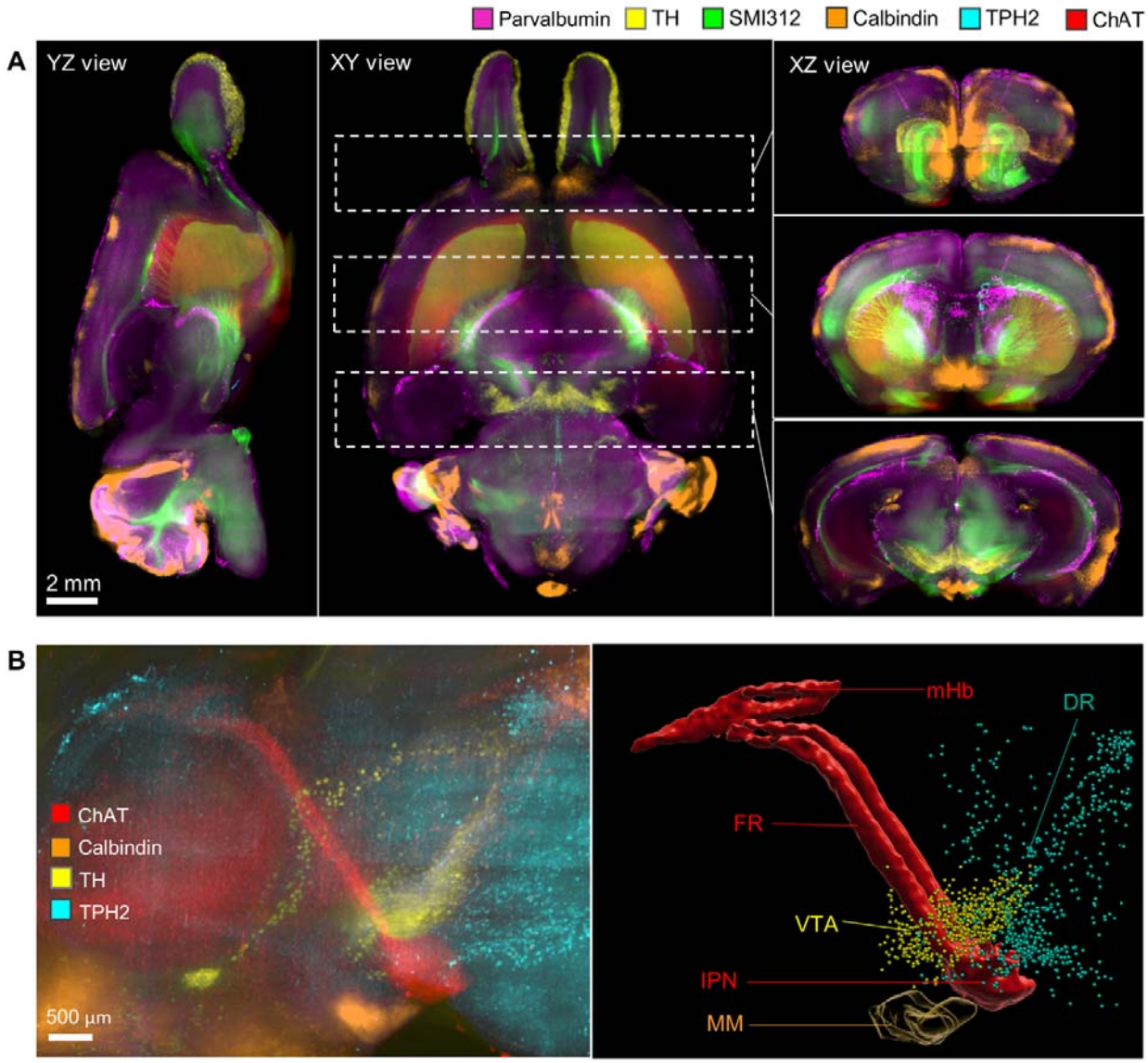

Figure 4. Merged multichannel neuron circuitry image generated by MOCAT+.
(**A**) Merged multichannel image generated using the datasets from Fig. 3. Optical sections from the horizontal (XY) and sagittal (YZ) perspectives are presented. For the transverse (XZ) views, projection images of the regions encompassed by the dotted lines in the XY view are displayed. (**B**) The spatial relationship of the Hbn-IPN circuitry, dopaminergic (TH), serotoninergic (TPH2), and calbindin+ GABAergic neurons. Fluorescence (right) and segmented (left) images are shown. mHb, medial habenula; FR, fasciculus retroflexus; IPN, interpeduncular nucleus; SuM, medial mammillary area of the hypothalamus; DR, dorsal raphe nuclei.

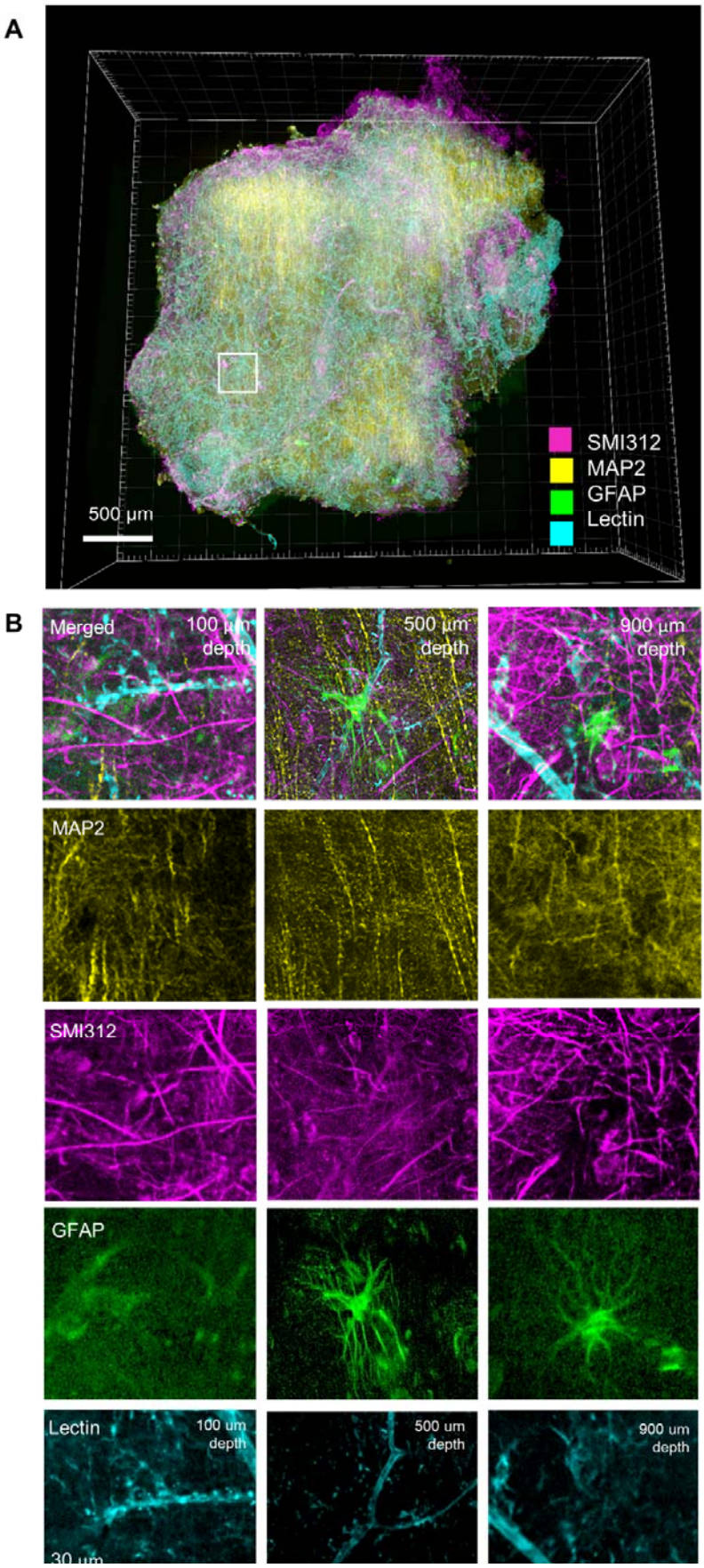
A
SMI312
MAP2
GFAP
Lectin
500 µm
B
Merged
100 µm depth
500 µm depth
900 µm depth
MAP2
SMI312
GFAP
Lectin
100 um depth
500 um depth
900 um depth
30 um

Figure 5. Multi-round immunostaining of a FFPE-MOCAT human brain specimen.
Three-round immunolabeling was performed on a FFPE human brain specimen collected from a patient with cerebral hemorrhage. Images were acquired using multi-point confocal microscopy.
(**A**) 3D rendering of the entire specimen.
(**B**) Images depicting merged and single channels of an optical section from the selected area (white frame) in (A) at depths of 100 μm, 500 μm, and 900 μm. GFAP: Glial fibrillary acidic protein; SMI312: pan-axonal marker; MAP2: microtubule-associated protein 2 (a dendritic marker).

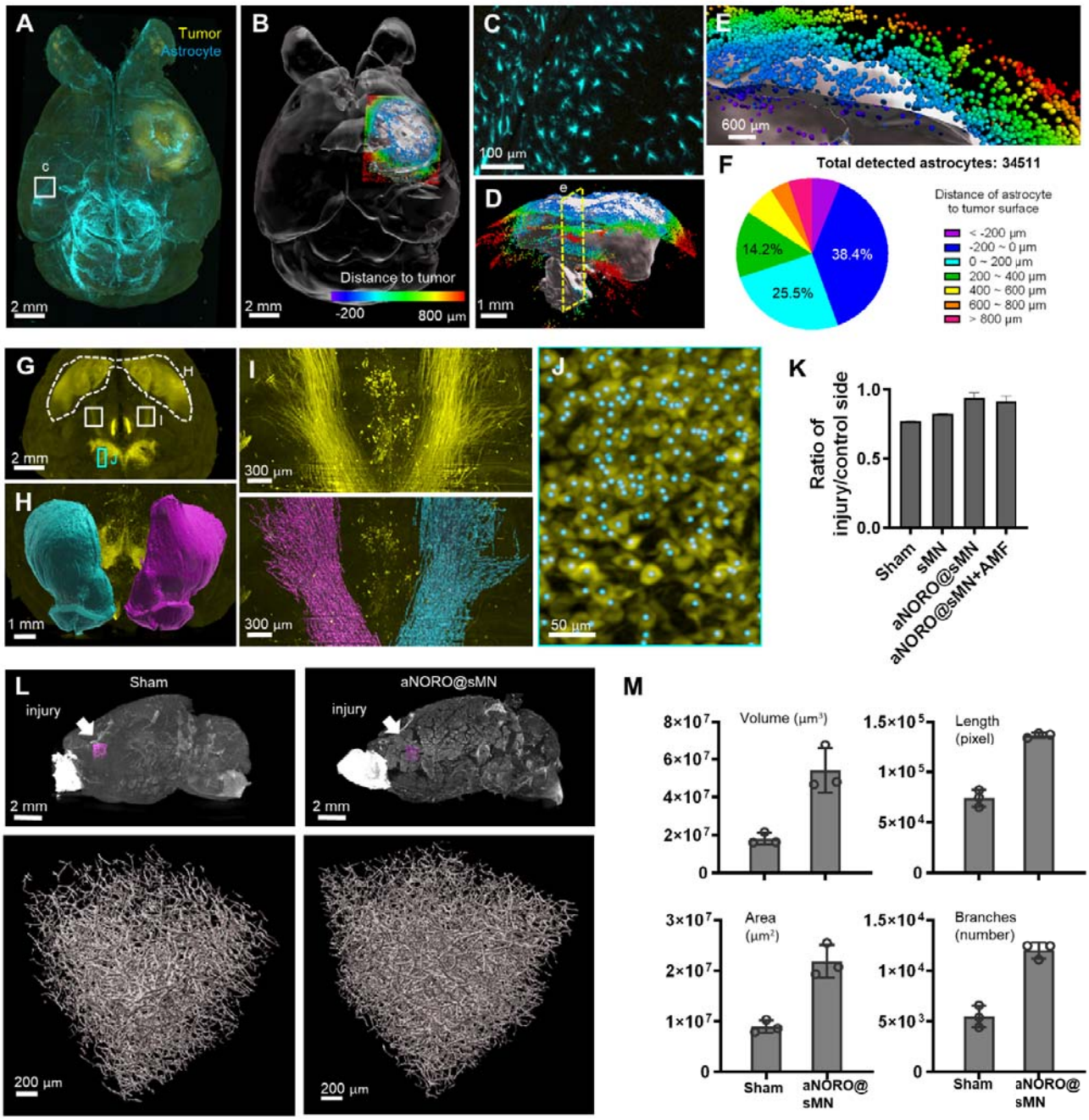
A
Tumor
Astrocyte
c
2 mm
B
Distance to tumor
-200
800 μm
2 mm
C
100 μm
D
e
1 mm
E
600 μm
F
Total detected astrocytes: 34511
Distance of astrocyte to tumor surface
< -200 μm
-200 ~ 0 μm
0 ~ 200 μm
200 ~ 400 μm
400 ~ 600 μm
600 ~ 800 μm
> 800 μm
38.4%
25.5%
14.2%
G
H
I
J
2 mm
1 mm
300 μm
50 μm
K
Ratio of injury/control side
1.0
0.5
0.0
Sham
sMN
aNORO@sMN
aNORO@sMN+AMF
L
Sham
aNORO@sMN
injury
2 mm
200 μm
M
Volume (μm³)
Length (pixel)
Area (μm²)
Branches (number)
Sham
aNORO@sMN

Figure 6. Applications of MOCAT in disease models.
(**A** to **F**) MOCAT reveals cell-tumor relationships in an astrocytoma model.
(**A**) Projection light-sheet image of a FFPE-MOCAT mouse brain with a GFP-expressing astrocytoma xenograft (ALTS1C1 cells, see Materials and Methods) stained for GFP (yellow) and GFAP (cyan).
(**B**) Segmented tumor (white) and surrounding astrocytes (colored). The astrocytes are colored according to the color-coded scale of cell-to-tumor distance.
(**C**) Magnification of the region marked in (A), showing astrocyte morphology.
(**D**) Sagittal view of the segmented tumor and color-coded astrocytes.
(**E**) Magnification of the clipping plane marked in (D, yellow dashed line), showing astrocytes inside (dark blue, purple) and outside (red, orange, yellow, green, cyan, blue) the tumor.
(**F**) Quantification of detected astrocytes and their classification according to distance to the tumor surface.
(G to M) MOCAT reveals brain damage and the therapeutic effect of alternating magnetic field-responsive NO-release octahedrons (aNORO) administered using a paracetamol-coated silk-based microneedle (sMN) in a TBI mouse model.
(G to J) Segmentation of dopaminergic regions in FFPE-MOCAT TBI mouse brains.
(G) Whole-brain projection light-sheet image focusing on TH-positive regions.
(**H**) Frontal view of the segmented striatum (dashed white line in (G)). Magenta: the injured side; cyan: the contralateral side.
(**I**) Horizontal views of the nigrostriatal fiber tract (paired white boxes in (G)); fluorescence (top) and segmented (bottom) images are shown. Magenta: the injured side; cyan: the contralateral side.
(J) Detection of dopaminergic cells in the substantia nigra (SN). Magnification of the marked area in (G), including the TH fluorescence signal (yellow) and segmented cells (cyan dots).
(**K**) Comparison of the therapeutic effects of different treatments. $n = 3$ (three indicators: striatum volume, nigrostriatal fiber tract volume, SN cell number), mean ± SD, * $p < 0.05$, ** $p < 0.01$, *** $p < 0.001$, **** $p < 0.0001$, one-way ANOVA with Tukey's multiple comparison test.
(**L**) Reconstruction of blood vessels in TBI brains with or without treatments. The regions of interest (ROIs) selected to assess angiogenesis are indicated in the top row (magenta boxes, directly below the injury site). 3D reconstructions of blood vessels are shown in the bottom row.
(M) Quantification of blood vessel volume, blood vessel surface area, number of blood vessel branches, and blood vessel length. $n = 3$, mean ± SD have been plotted.

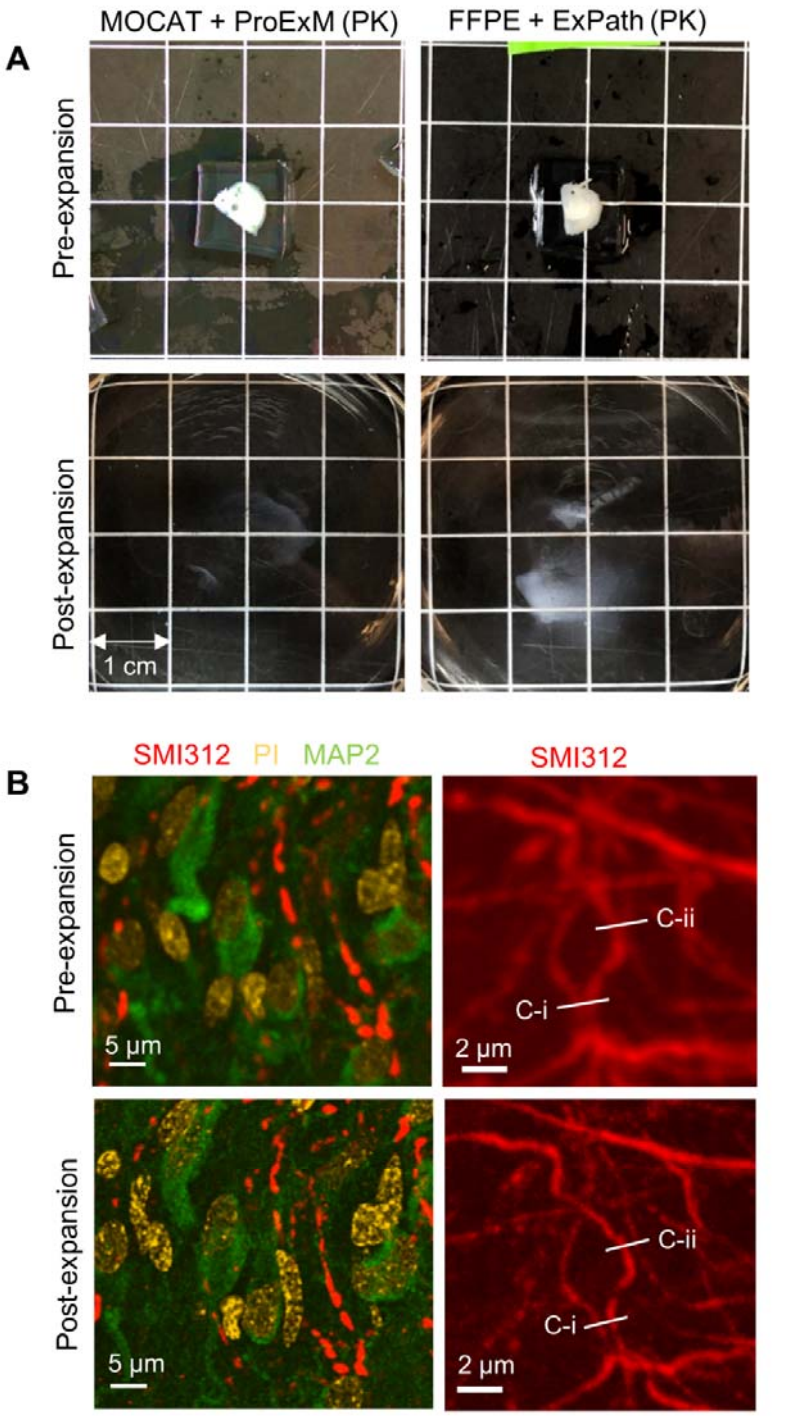
A
MOCAT + ProExM (PK)
FFPE + ExPath (PK)
Pre-expansion
Post-expansion
1 cm
B
SMI312 PI MAP2
SMI312
Pre-expansion
Post-expansion
C-ii
C-i
5 µm
2 µm
C
i
ii
Intensity (a.u.)
100
80
60
40
20
pre-expansion
post-expansion

Figure 7. Expansion microscopy on a FFPE-MOCAT human brain specimen.
(**A**) Gross views of expansion of a 1-mm FFPE specimen.
(**B**) Fluorescence images of a FFPE human brain pre- (top row) and post-expansion (bottom row). Left: merged images of multiplexed staining; right: fluorescence images of SMI312 staining.
(**C**) Profiles of axon signal intensity taken along the white lines shown in the images of the right panel in (B). The scale bar has been divided by the expansion factor.